Simulating Atmospheric Haze for Image Degradation Analysis

Michael W. Scruggs

Master's Report

College of Optical Science

University of Arizona

Spring 2015

Prologue:

This following report shows an overview of the work done to fulfill the writing requirement for the University of Arizona, Optical Science Master's program. This research report is not traditional of the average master's student. However, the overall purpose of this assignment is universal to the standards of the University of Arizona; prepare students for successful careers post-graduation. In selecting a topic, it was imperative to align with my future position as a Naval Surface Warfare Center scientist. This was accomplished by learning about and attempting to use polarization as a means of altering image contrast. The educational exercise aspect of the report included defining a simple problem and progressing from that initial vague solution to a fully developed and accurately simulated final solution. Over the course of this academic exercise, all steps of the systems engineering process were experienced. The first step of the process involved defining loose requirements that would be used throughout the exercise. By next simulating expected results, final requirements were developed from the expectation of how the system would operate under the stress of the real-world environment. Errors and uncertainties were incorporated into the simulations. Preliminary (PDR) and critical (CDR) design reviews were incorporated into this academic exercise to simulate the real-world experience of costumer and engineer interaction. The PDR exposed the costumer to the initial system design. Explanation of the system occurred during this phase and was followed by customer feedback, comments, and concerns. These comments and concerns were addressed and the initial system progressed towards a final operational system. After solidifying the design, the final CDR was used to demonstrate the updated design that in theory would be ready to manufacture for final testing and analysis. By following the final design, an optical system was fabricated and tested under laboratory conditions. The report designed the developed system along with an analysis of the system results. The entire process was tailored to the purpose of becoming familiar with all the steps involved with taking a raw idea through the entire engineering process. By experiencing this process from start to finish, many real-world problems were experienced. The non-traditional aspect of this report involved the difficulties and lessons learned that would not traditionally be included in a scientific document. A large portion of this exercise is not listed in the report, but positively influenced the overall success of the assignment. Difficulties existed in making the system operate in the same manner as the simulations. Also, difficulties existed in collecting the equipment necessary to build the optical system. It was important to experience all aspects of the design and trouble shoot through the problematic spots while maintaining a "swim or drown" attitude towards the assignment. The experience gained from adapting and solving these unforeseen circumstances will transition to a more successful career. Overall, the main goal of experiencing how even the most trivial designed can become complicated and difficult without proper planning and thinking through all aspects of the design was met. I would recommend any graduating student be exposed to the system design process from start to finish along with official PDR and CDR meeting at some point in their academic career. The experience and guidance demonstrated from committee members will benefit all students involved immensely and should not be over looked.

Outline

Abstract:
The effects of polarization have been widely demonstrated and proven beneficial in many applications in the medical, military, and private fields. It is commonly used for image discrimination, as certain objects alter polarization properties of light upon reflection. Polarizers are used to block specific polarization states, while retarders are used to alter polarization states. These elements can be used to selectively block unwanted light and improve image quality. This report involves imaging through haze conditions in the atmosphere. By exploiting polarizing properties caused by atmospheric Rayleigh scatter, algorithms have been developed to remove the atmospheric polarized light from the total light irradiance of the object source. (Schechner, 2003). Simulations and experimental validation were performed based on Schechner's research. This process involved data collection, processing, and light removal. Modulation transfer functions were utilized for analyses of performance. Results were compared to theoretical simulated error. Laboratory created atmospheric conditions were proven to produce partially polarized light by way of Rayleigh scattering. Three different object sources were imaged through the simulated atmospheric conditions to analyze the system. As particles in the simulated atmosphere became more dense image quality degraded. Post processing efforts to regenerate image quality utilizing Schechner's calculations were unsuccessful based on the limited scale of the experimental set-up.

I. Introduction

Atmospheric haze has negative implications on image quality. As seen on any foggy day, the introduction of particles along the light path causes scatter and reduces image contrast. By selecting certain orientations of polarization to block and pass light, image quality can be partially restored. Mastery of these concepts can open many doors to government, public and private industry. Polarization is used for image discrimination, as certain objects alter the polarization orientation of light upon reflection. By selecting the particular orientation of polarized light you wish to collect, object contrast can increase and decrease within a scene. Prior work indicates that illumination sources (sun, incandescent bulb, moon, etc.) produce random "un-polarized" light. This does not suggest that polarization properties do not exist, but these properties are equally weighted within the overall light distribution. Selective image collection methods and post-collection image processing can produce fully-polarized images, as well as, reduction of polarization effects from an image. Polarizers and retarders are used to isolate certain polarization orientations from all other light wave information giving polarized light data. With knowledge of polarizing properties in the atmosphere, algorithms have been developed to remove the atmospheric polarized light from the total light irradiance of the object. Experimental analysis was done to mimic the previously completed analysis of removing atmospheric polarized light created from Rayleigh scattering in haze to regenerate image quality (Schechner, 2003).

Figure 1 below illustrates the designed system. Illumination system #1 illuminates the object. By positioning the light behind the object and reflecting off the rear wall, back-lit illumination is produced. By illuminating the object directly, front-lit illumination is production. A tank of water is positioned between the object and imaging system. This tank of water has a separate illumination system #2. Particles will be added to the tank and illuminated to simulate atmospheric haze conditions between object and image. The imaging system will be used to collection light information from the object. This system includes a polarizer, entrance pupil, lens, and detector.

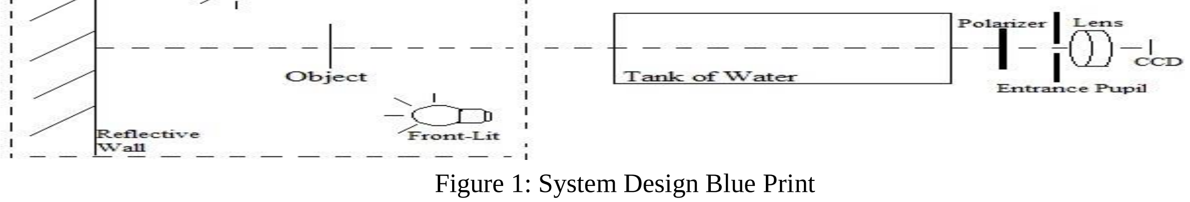

Figure 1: System Design Blue Print

A requirements section was created to define all specifications of the optical system. Simulations were done to calculate anticipated error. Error allocation was implemented to define which portions of the system will be most likely to impose loss in image quality. The final step was manufacturing a full system designed in regards to the anticipated performance level. This system was constructed based on the design above. The system was analyzed for performance and compared to theoretical predicted error sources. After meeting all operating requirements, the optical system was incorporated into the overall experiment to map an object through simulated haze. Simulated haze is created by adding particles, milk, to the tank of water and illuminating the tank. An assumption is made that scatter produces polarized light. The polarized light propagated through the tank interacted with the random light from the object. By utilizing a linear polarizer, polarized light was collected, processed, and removed to reduce the effects of scattering. This experiment mimicked a real-world application of polarization for enhancing image quality. By suspending particles in air or water, scattering and image degradation is caused; however, selectively separating polarized light from random light allows for imaged regeneration.

II. Theoretical Expectations

The experiment developed by Schechner, Narasimhan, and Nayar, *Polarization-Base Vision through Haze*, 2003, was the driving force for this master's report that utilizes the removal of a select orientation of polarization for image regeneration. The paper will be addressed followed by defining the type of scatter occurring within the system. After establishing background information for the experiment, the system requirements and method of evaluation will be discussed. Simulations will be used to justify the requirements. The data collection method for experimentally analysis will finalize the theoretical expectations.

Polarization-Base Vision through Haze

The premise of the analysis by Schechner, Narasimhan, and Nayar originated from the idea that partially polarized light is the byproduct of atmospheric scattering from natural illumination. The analysis concentrates on the following calculations for selectively removing the naturally polarized light. Image processing is used to reveal assumed unpolarized, random object source information passing through the visually hazy conditions from atmospheric scattering. *Airlight* is scattered illumination between object and image. The amount of airlight will grow with respect to an increase in distance (z) between object and image. Beer's Law is used to express the degradation of object light in the atmosphere when haze is not present. This is represented by the coefficient β. The β-term changes with distance and must be integrated, Eq. 1.1. In the unique case where β operates independently of distance, Eq. 1.2 is used. Airlight maximum (A_{max}) is the airlight value per pixel for an assumed object at infinity. The value can be derived using several methods depending on atmospheric conditions and distance. For Schechner's analysis, the simplest method was used. An image is collected through haze conditions of the sky just above horizon without the presence of an object scene. A_{max} will be used to define the total airlight.

Equation 1.1: $t(z) = (1) \ \ \exp\left[-\int_0^z \beta(z')dz\right]$ Equation 1.2: $\exp(-\beta z)$

Equation 2: $A = A_{max}[1 - t(z)]$

Airlight (A) will be redefined using the following terms. $A^{\perp}$ represents perpendicular light scattered from solar illumination. $A^{=}$ represents parallel scattered light. The terms $A^{\perp}$ and $A^{=}$ are scatter dependent and will switch dominance in the total Airlight irradiance depending upon the particle size in the atmosphere. $A^{\perp}$ is dominant when the Rayleigh scattering criteria is met, while $A^{=}$ is dominant when Mie scattering is met. Polarization is defined by the scattering angle (ɵ) that exists between the sun illumination and the optical axis. Polarization (p) is represented using the follow equation:

Equations 3: $p \equiv \frac{(A^{\perp} - A^{\parallel})}{A} = \frac{sin^2\theta}{1+cos^2\theta}$

An assumption is made that the total light distribution from the object (L_{obj}) is unpolarized. The total light (I) from the object after transmission loss is shown in the following equation.

Equations 4: $L = L_{obj} * \mathrm{t(z)}$

Total light, defined by the term I_{total}, is the sum of A and L. With the addition of a linear polarizer to the optical system, the value of I_{total} will diminish based on blocking certain orientation of polarization. The following procedure is the mainstay of the analysis. Angle (φ) represents the first angle of polarizer that is positioned around the optical axis. By emphasizing certain polarizer angles, L becomes dominate over A. As previously stated, object light is random. Therefore partial light from the object will be blocked by the polarizer. When selecting φ, the user will evaluate maximum visible reduction of irradiance and collect an image. This image represents the "ideal," $I^{=}$. The "non-ideal," $I^{\perp}$, will be an image collected at φ ± 90º from $I^{=}$. Theoretically, this image will pass all linear polarization components previously blocked. The following figure shows that I_{total} changes as a function of polarizer orientation angle.

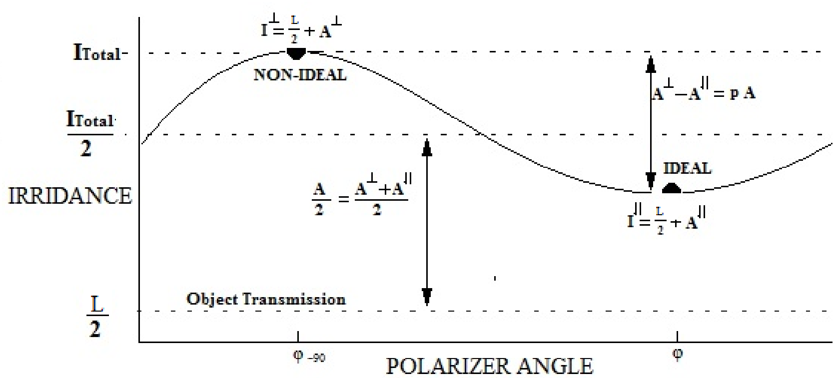

Figure 2: Sinusoidal Relationship between Non-Ideal and Ideal Polarizer Orientation

After collecting an image at ideal and non-ideal angles, calculations and image processing are used to produce a final image that emphases object light. The following steps illustrate removal of airlight from the experimentally collect irradiance data, $\dot{I}_{otal} = \dot{I}^{\perp} + \dot{I}^{=}$. There will be an equal loss in irradiance from the object scene in both images. Two equations are derived to split the distribution of polarization.

Equations 5: $I^{\perp} = \frac{L}{2} + A^{\perp}$ | $I^{=} = \frac{L}{2} + A^{=}$

By redefining terms $A^{\perp}$ and $A^{=}$ (Eq. 3), the terms can then be incorporated in the polarization equations above.

Equations 6: $A^{\perp} = \frac{A(p+1)}{2}$ | $A^{=} = \frac{A(p-1)}{2}$

Back calculations are required to transition from the collected $\dot{I}^{=}$ and $\dot{I}^{\perp}$ images to object irradiance. The irradiance of each pixel includes unknown object ($\acute{L}_{obj}$) and airlight ($\acute{A}$) irradiance. The effects of atmospheric transmission ($\dot{t}$) are also unknown. Since airlight is also affected by transmission with respect to distance, these two unknown values are evaluated in unison. The following equations are used to determine the $\acute{L}_{obj}$ by removal of airlight properties.

Equations 7: $\acute{A} = \frac{(\dot{I}^{\perp} - \dot{I}^{\parallel})}{p}$ | $\acute{L} = \dot{I}_{total} - \acute{A}$

A computation program is required for this image analysis as each pixel is processed separately. The effects of polarization will vary from one pixel to the next. Objects of increased distance will show increased variation between pixels. The final result is an irradiance value per pixel dominated by the raw object irradiance.

Scattering

This phenomenon occurs when a light wave encounters particles. An assumption that elastic scattering occurs will be required for analysis. In elastic scattering, kinetic energy is conserved; however, the direction of propagation changes. The alternative form of scattering is inelastic. In this case, the particles are larger than the wavelengths interacting with them. Therefore, the energy of the smaller waves is not completely conserved. The two main types of elastic scattering are Rayleigh and Mie scattering. The radius of particles (r) and wavelength of radiation (λ) define the two types of scatter. The following equation addresses the particle size by a single dimensionless value, x.

$$\text{Equation 9: } x = \frac{2\pi r}{\lambda}$$

Rayleigh scattering is defined as scattering when the particles are smaller than the wavelength of radiation acting upon them, $x << 1$. Mie scattering is scattering that occurs between spherical particles that are roughly the same size as the wavelength of radiation acting upon them. This occurs when $x \approx 1$. Mie scatter is still considered elastic as the majority of energy is conserved; however, polarization properties that exist from Rayleigh scattering disappear within the realm of Mie Scattering. Any x-value greater than 1 is described as Geometric scatter. As particle size increases, geometrical optics methods are used to define the effects on electric field (Arai, 2013). The important different between Rayleigh and Mie scattering is the angle of energy propagation that results from the interaction of particle and electric field. In Rayleigh scattering, light is dispersed in all directions except 90º, as illustrated below. Mie scattering yields greater scatter occurring in the propagation direction of the original electric field. The larger particle size makes the deviation of electric field from the original path of travel more difficult. The following figure is used to represent the angular scattering difference between Rayleigh and Mie scattering.

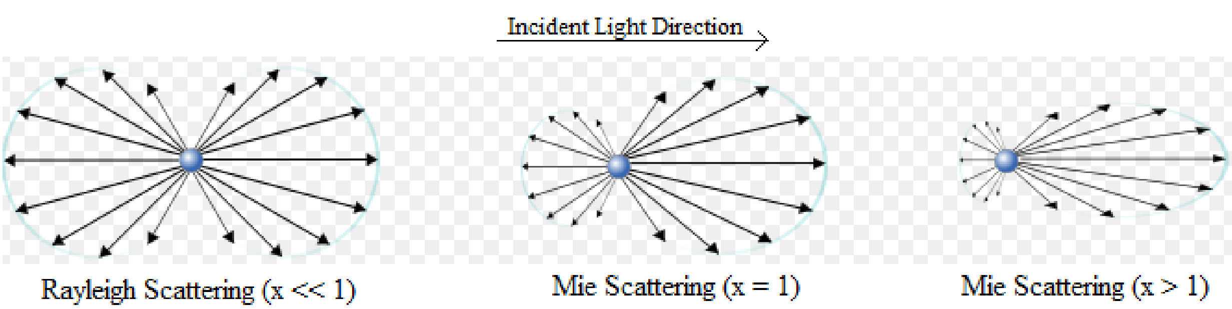

Figure 3: Angular Scatter Distribution Comparison of Rayleigh vs. Mie Scatter

System Quality Evaluation

The following terms are used to evaluate the system being designed. Airy Pattern (AP), this is a phenomenon of diffraction that occurs when light passes through a circular aperture stop of an optical system. Upon passing through, diffraction occurs as the wavefronts interact with the stop. The result is a bright central core that includes the majority of the power. Rings of lower irradiance will surround the central core. The spacing of the rings can be calculated using a Bessel equation in conjunction with system specifications including working f-number and wavelength of radiation. Strehl Ratio (SR) is a single value measurement of image quality. The value can range from 0 to 1. An ideal AP will be normalized to 1 (E_0). The normalization occurs at max irradiance found at the peak of its central core. The AP produced from the evaluated system (E_0') will be assessed with respect to the AP produced from the ideal system. Inconsistencies in the evaluated system will result in a value less than 1. By using the equation below, a Strehl ratio can be calculated for an AP of interest.

Equation 10: $Strehl\ Ratio = SR = \frac{E_0'}{E_0}$

A Point Spread Function (PSF) is the image of a point source. The Airy Pattern above would be considered a PSF as it is the response of the system to light from a point source. By imaging a point source, the user is effectively imaging a delta function. Diffraction occurring at the entrance pupil causes the deviation of light that produces an image on the sensor. Ideal systems will produce an AP. The AP image will deteriorate when aberration effects are present. A Transfer Function (TF) is used to describe the way an object is altered as it passes through an optical system. An object can be broken down into individual sine waves that describe the object. These sine waves are individually imaged by an optical system. The output sine waves have an identical frequency to the input sine wave; however, each sine wave may have different amplitude (A) and phase term (ω). By summing of all the output sine waves, an image is regenerated. A perfect optical system will map an input to an exact replica output; however, diffraction, aberrations, and element quality make this impossible.

A Modulation Transfer Function (MTF) represents the amplitude change of the transfer function as it varies with respect to frequency. This is done taking by taking the magnitude of the transfer function and normalizing all values with respect to the amplitude occurring at a frequency of zero.

Equation 11: $\mathrm{MTF} = \frac{|\Im\{\mathrm{PFS}(x', y')\}|}{|\Im\{\mathrm{PFS}(x', y')\}|_{x'=0; y'=0}}$

Requirements

The first requirement is that the system shall be diffraction limited. The system shall produce a minimum Strehl Ratio of 0.8. This is the most important aspect of the system design. By requiring that the system be diffraction limited, the airy central core disk must contain a minimum integrated energy of 80% of the total irradiance entering the system. The remaining 20% of irradiance will be distributed throughout the airy pattern, outside the central core. The second requirement is that the Airy Pattern central core diameter shall have a width greater than 10 pixels. The diameter may not exceed 2.0% of the detector width. This requirement has been established so that the AP core will be large enough for effective sampling while small enough to result in high spatial frequency information. Finally, requirement three is that uniform illumination shall exist across any object of interest. The irradiance shall not decrease by more than 5% across the object.

Simulations

Prior to system design, simulations were conducted to mathematically reproduce error that will inevitably exist based on the inability to build a perfect system. By doing such, error can be allotted to different aspects of the design giving the design a realistic expectation for performance before manufacturing a prototype. Three errors were simulated. Each error shows the amount of imperfection that could exists based on the requirements above. By establishing the different sources of error that will exist, the manufactured system with have a more realistic theoretical expectation.

The error resulting from the first requirement was realized by simulated an Airy pattern. The cylinder (cyl) function in MATLAB was used to mimic a cylindrical entrance pupil being used in the system. Using the Discrete Fourier Transform (DTF) command, the simulated effects of diffraction were applied to the created cylinder function as light passes through the entrance pupil. This produced a sombrero function which represented the electric field (EF) pattern because the object source was producing incoherent wavefronts. The irradiance was calculated by taking the magnitude of the E-Field and squaring the results. The equation below illustrates the previous written explanation.

Equation 12: $$\left|\Im\left\{cyl\left(\frac{r_p}{D_{EP}}\right)e^{\frac{i2\pi\omega(x,y)}{\lambda}}\right\}_{\xi=\frac{x}{\lambda f'},\eta=\frac{y}{\lambda f'}}\right|^2$$

Variables within the above equation include radial pupil coordinates (r_p), entrance pupil diameter (D_{EP}), and wavefront error (ω). X and Y represent the linear space coordinates while ζ and η represent the frequency space coordinates. For this simulation, the wavefront error was set to zero; however this term would be used to assess aberrations and errors in the wave front traveling through the pupil. After creating an AP, the irradiance value at the center of the pattern was divided by that of an ideal AP to produce a Strehl Ratio value. The figure below shows an AP at the minimum acceptable Strehl Ratio value 0.8 (blue) plotted against theoretical AP (red).

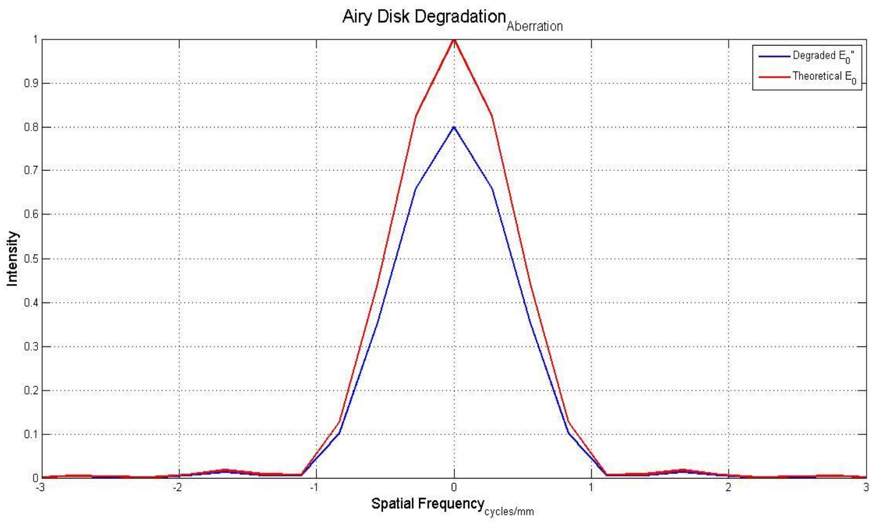

Figure 4: Theoretical Airy Pattern and Minimal Air Pattern by Strehl Ratio

Error from the second requirement was found by analyzing an Airy Pattern of central core diameter less than 10 pixels wide. To analyze this requirement, the AP creation method remained consistent from the previous section. The simulated entrance pupil diameter (D_{EP}) was adjusted to alter AP diameter as seen in figure 5. The two working domains, linear and frequency, act as inverse to one another. By selecting the appropriate range of D_{EP} (0.5-1.2 [mm]), simulations were done to select the acceptable range of 15-30 pixels. By specifying the width of the airy pattern in pixels, the airy pattern irradiance will cover enough pixels for accurate imaging while being small enough to produce high spatial frequency information.

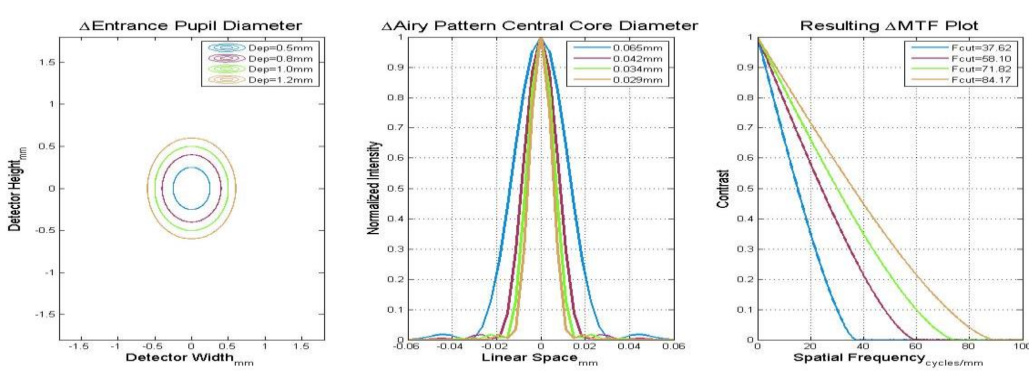

Figure 5: Different Size Entrance Pupil Effect on Airy Pattern and MTF

The object will be uniformly illuminated with a nonuniformity of 5%. This is used to address the third requirement. Consistent irradiance is necessary when mapping an object through an optical system. Image degradation will occur as a function of uniformity loss. Simulations were performed to determine the acceptable loss in uniformity as a function of resulting degradation in MTF. Since the experimental pattern of illumination degradation is impossible to predict and even more difficult to accurately simulate, a simple quadratic equation was used to map illumination roll-off from the center of the object outward. The following figure shows the simulated decrease in irradiance across an edge function. The resulting MTF plots illustrate a variation in contrast at low frequency values. The nonuniformity that occurs away from the cut-off of edge causes this sinusoidal ringing and MTF plots that do not appear to normalize.

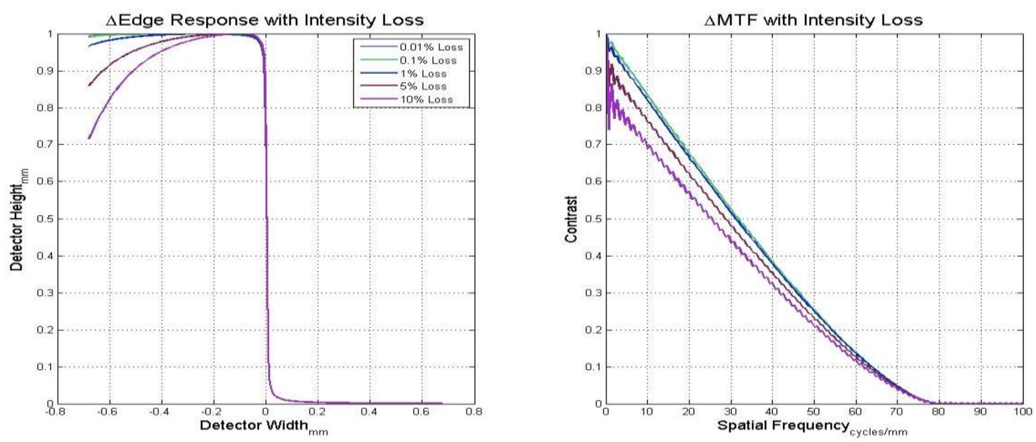

Figure 6: Effects of Light Irradiance Roll-Off to Edge Response MTF

Data Collection Methods

For this experiment, the measureable characteristic of the light is the irradiance on the detector. The detector used for the experimental process was monochrome and capable of detecting light within the range of 0.3-1 [μm]. Transmission filters were used to block particular wavelengths of light from entering the detector. This experiment incorporated a Near-Infrared (NIR) Filter that allowed light radiation of 0.7-2.0 [μm] to pass. The camera has 2.5x2.5 [μm] pixels. After using the detector for data collection, image processing was done for characterizing the experimental success. MATLAB was used to perform all necessary image processing. Three different object sources were used to produce the images for processing. Each will be addressed in the experimental section.

VI. Experimentation

The goal of the experimental process is to cause predicted degradation to the MTF. The measured changed to the MTF are expressed in the results section. The system consisted of an imaging component that was used to image three object sources. A tank measuring 300x150x200 [mm] will be placed between the image and object locations along the optical axis. This experiment included three different set-ups. The first experimental set-up, System 1, was the experimental constant. The tank was filled with water; however, no scattering properties were added to the water. The second set-up, Systems 2, included scatter in the tank. Milk was added to the tank in increments of 15 [ml]. The third set-up, System 3, included scatter in the tank in the same increments as System 2. System 3 involved the addition of a polarizer for polarization passing ability. The first variable for the experiment was the amount of milk added to the system. The second variable will be a linear polarizer added to the optical system.

Systems

The systems imaged an object from a fixed location through the optical system producing an image on the detector. For each system, the tank was filled with water and positioned between the object and optical system. Tank Illumination System was exposing light irradiance to the water within the tank. The halogen broadband source introduced incoherent light to the system. The source produced a large range of wavelengths. The Tank Illumination System remained on, as it was constant throughout the experimental process. This set-up was used to verify the optical performance compared to the theoretical design. System 1 was used to compare the degraded performance of System 2 and 3 to the ideal conditions without scatter.

System 2 degraded the image quality. Properly sized particles were added to the tank in increments of 15 [ml]. Fat Free Milk was used because the size of the particles matches the necessary specifications. Milk consists of spherical lipids that contain fat and vitamin molecules. The size of lipids range from 0.1-15 [μm]. Fat Free milk was selected because the majority of lipids have a diameter less than 0.2 [μm] (Coulter, nd). The small size of the particles will yield a greater chance for Rayleigh scattering to dominate. By increasing the amount of particles present in the tank, the image quality should degrade.

System 3 was identical to System 2; except a linear polarizer was added in front of the optical system. Angles of 0°, 25°, 45°, and 90° were used for image collection where 90° is the polarization pass direction. Based on the paper by Pomozi, 2001, the polarization via Rayleigh scattering from the tank is expected to produce linearly polarized light ranging from 0º to 45º with respect to the optical axis. Scatter effects from the tank should be reduced based on the polarizer angle.

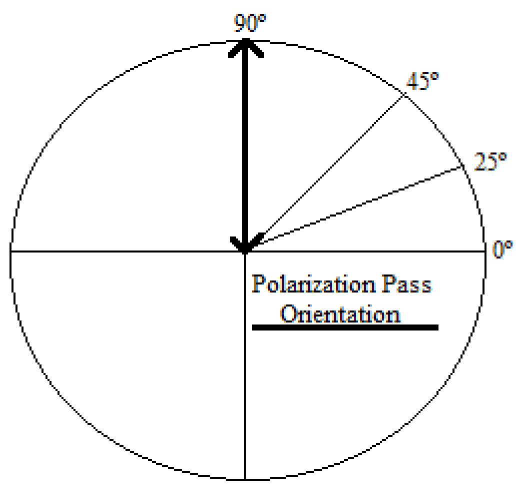

Figure 7: Polarization Orientation

Object

Each system set-up imaged three different objects. A Point Source, Edge Source, and Resolution Star were imaged. A red diode laser (670 nm) was used to produce a point source. The laser was completely blocked from the optical system except for a circular pinhole of 0.5 [mm] diameter positioned 10 [mm] in front of the laser. This object mimicked a delta function and produced an impulse response on the detector. By using a point source object, a radially symmetric MTF can be calculated. Noise is a likely source of error associated with this objects because DC off-set can affect MTF. Dark images were captured from the detector without the presence of light prior to experimentation. The edge was produced by using a black, opaque, plastic square. The object was setup perpendicular to the optical axis that will hypothetically pass through center of the edge. Uniform illumination and noise reduction are important to the system as they affect image quality. The method of back-illumination was selected for this experiment. The Object Illumination System was set-up off the optical axis and behind the object with respect to the optical system location. White paper was illuminated behind the object location and light was reflected toward the edge and detector. This illuminated the rear-side of the edge object. Uniform irradiance occurs from his method, but the magnitude of irradiance was reduced. The edge presented the optical system with a cut-off between illuminated and non-illuminated areas. A cross-section of the edge image perpendicular to the illumination cut-off was used to calculate the Line Response (LR) in linear space. The LR(x,y) is found by takin the derivative of the edge cross-section. The benefit of this derivation is the removal of constant irradiance counts from the dark (edge) and bright light (no edge). The MTF of the Edge will be used as a second method of characterizing the system performance.

The final object was a resolution target. The front illumination method was used for the resolution target. With the target placed at a specific conjugate distance, an image was collected of the target. By determining where any two lines (white and black) are no longer resolvable, the quality of the system resolution can be expressed. This is used for additional contrast and resolution information. For experimental purposes, the Resolution Star below will be used as an object. System assessment by this means will be qualitative.

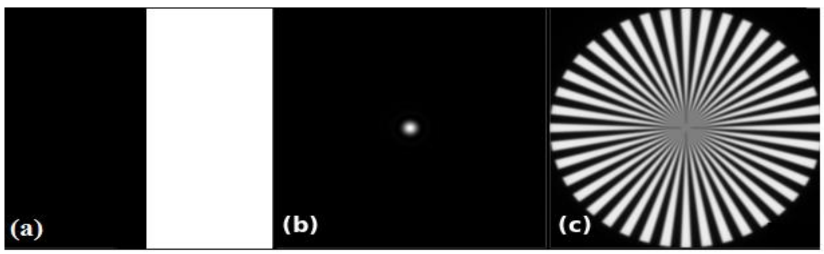

Figure 8: (a) Edge, (b) Point Source, and (c) Resolution Star Target

System Design

After simulating system requirements, the system specifications were selected to produce a system with minimal error. The errors associated with each requirement were combined to determine the expected error. The success of the system was determined by comparing the experimental Modulation Transfer Function and the theoretical. The focal length (f_e) was selected to be 45 [mm]. This gives the appropriate power to effectively map objects of radially size 300 [mm] at a distance of 3000 [mm] to the image plane which is roughly 5.3x4.0 [mm]. The focal length was selected to assure that enough space was allowed between the lens and detector for focusing the system. The Entrance Pupil Diameter (D_{EP}) was selected to be 1.0 [mm]. An adjustable iris was used for the entrance pupil. The focal length and entrance pupil yield a working f-numer of f/45. The object distance was 3500 [mm] and the wavelength range was 0.7-1.0 [µm]. The f_e and D_{EP} will completely define the optical system, as working focal length (F/w), AP diameter (D_{air}), and frequency cut-off (F_{cut}) all depend on these variables.

Equation 13: $F/w = \frac{f_e}{D_{EP}} \quad ; \quad D_{airy} = 2.44\lambda f_{\#w} \quad ; \quad F_{cut} = \frac{1}{\lambda f_{\#w}}$

There two key attributes of the sensor include sampling rate and Nyquist frequency. Sensor size is 2080x1552 pixels. The pixel size will directly correlate to the maximum sampling rate (f_s) of 400 [cycles/mm] with a Nyquist Frequency (N_f) of 200 [cycles/mm].

Equation 14: $f_s = \frac{1}{Pixel\ Size} = \frac{400\ cycles}{mm} \quad ; \quad N_F = 0.5 * f_S = \frac{200\ cycles}{mm}$

After the sampling rate has been established, the importance of the wavelength range sampled can be addressed. The wide range of detectable wavelengths caused the AP to change with respect to each wavelength represented in the halogen light source. The individual wavelengths will have different focusing distances because of the lens element dispersion. A Near Infrared Filter was used to limit the spectral range passed by the system to 0.72-1.0 [µm].

VII. Results

Ideal System Analysis

The original designed system was to operate as an f/45 system; however, the initial design was built as an f/72.6 system. The larger working f-number caused a slower system, allowing less light to enter the system. The entrance pupil was set to 0.62 [mm]. The theoretical cut-off frequency is 20.6 [cycles/mm]. This change to a slower system was done to restrict additional light into the system. Upon experimentation with the object illumination systems, the image was not bright enough even without the presence of scatter in the system. By using a larger working f-number, image distinction was impossible. In the edge response section below further adjustments to the initial system are explained. The hope was for more distinct image contrast under the presence of scatter in the system.

PSF: The experimental AP central disk width measured 0.114[mm] which corresponds to 45.6 pixels across the detector. The simulated theoretical AP central disk width measured 0.116[mm]. The percent error of the AP is 1.7%. The theoretical MTF data was simulated in ZEMAX for the lens used in the experiment. Two ways to characterize difference in MTFs includes comparison of the cutoff frequencies and difference in contrast at a determined contrast value. Analysis of the f_c showed the system to cut-off at a frequency slightly lower than the allowable cutoff frequency of 18 [cycles/mm]. The theoretical MTF at 0.5 contrast value corresponded to a frequency 8.4 [cycles/mm]. The experimental MTF measured 0.45 contrast at that frequency. The percent error was 13.4%. The allowable error in contrast was 12.2% determined during the design phase. The Airy Pattern central disk was used for the final analysis of the MTFs. This revealed that the percent of integrated energy under the disk was 91.4% of the theoretical. This value proves the requirement that system shall be diffraction limited.

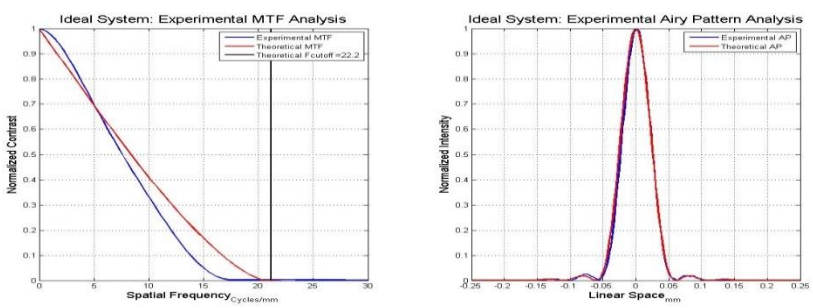

Figure 9: Experimental MTF and AP Plots for the Ideal System Set-Up

Edge Response: Errors in the initially constructed system were found during the edge response analysis. The slow nature of the F/72 system would not allow a detectable level of irradiance to pass. The iris was removed from the system altering the working f-number to F/1.8. Results were collected for the plastic edge under back-lit conditions and the front-lit condition. However, both back-lit and front-lit illumination produced noise across the dark edge to bright no-edge boundary. The non-uniformity that existed across this boundary resulted in noisy MTF measurements, as seen in figure 10. By altering the illumination set-up, the hope was to produce uniform illumination and reduce noise. Another alteration occurred by changing the number of tungsten filament sources. The irradiance was increased with this change; however, the uniformity remained sporadic. The increase in irradiance produced an increase in noise from wall and paper reflections in the black-lit set-up. The increase in irradiance caused the front-lit system object illumination to increase but the result was still non-uniform irradiance. After altering the magnitude of irradiance from one halogen source to four equally spaced sources, the distance of these sources away from the object was also varied. By moving the illumination sources away from the object, the image looked more uniform. The corresponding MTF B showed unreliable information. Figure 10 shows three different experimental set-ups and the resulting MTFs. The first figure, A, shows the initial front-lit illumination method of the computer printed edge with an entrance pupil diameter of 1.5 [mm]. The second image, B, shows the front-lit computer paper edge with the illumination set-up moved away from the object. The entrance pupil diameter was opened to increase light into the system. The third image, C, shows the back-lit plastic edge object. These initial collections showed the difficulties in finding a good balance between object illumination and MTF measurements.

Figure 10: Edge Response of Different Experimental Set-Ups

Analysis suggested that removing noise from the collected results would be required to use the data. By averaging

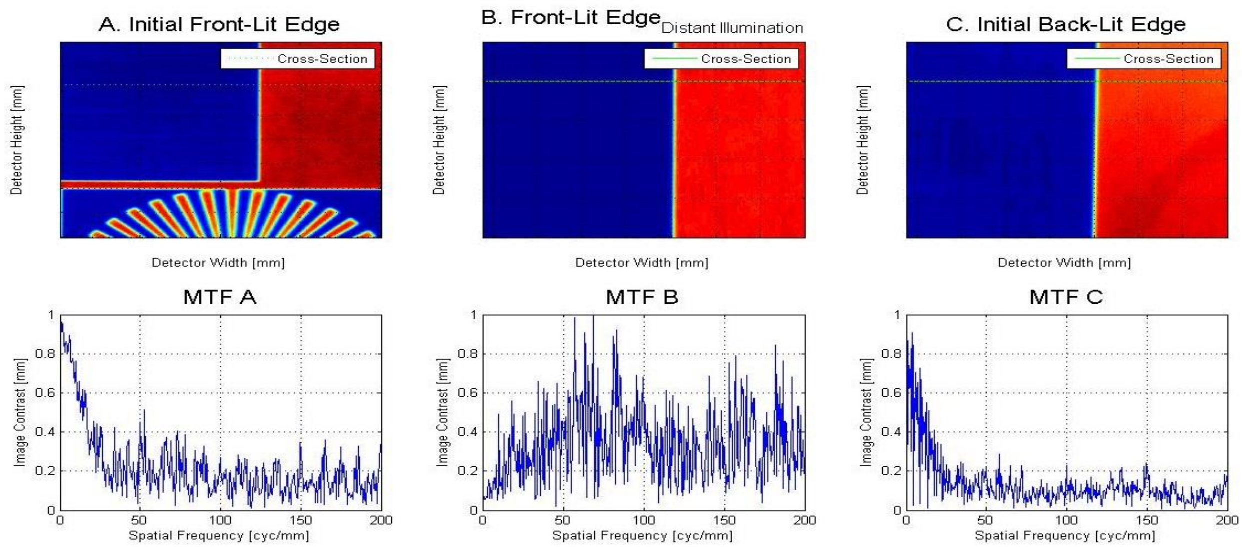

10 images collected in sequence, the noise associated with the front-light edge object was diminished. These results are shown in the figure below.

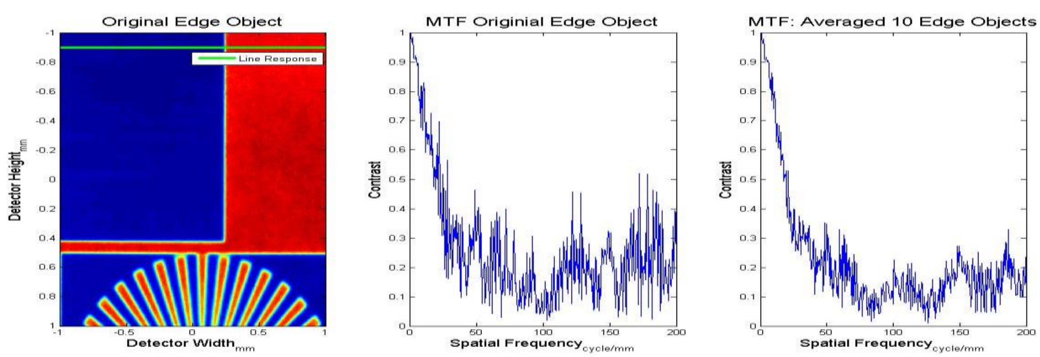

Figure 11: Decrease in Noise Response from Image Averaging

Resolution Star: The resolution target was imaged by the system for qualitative analysis. Original front illumination methods were used on a printed object. Mathematical processing and evaluations were not performed on this image. The star was analyzed visually by the user to evaluate image quality in real time. The following figure shows the system response to the star object that is used in later comparisons as the image will degraded to due scattered light present in the system.

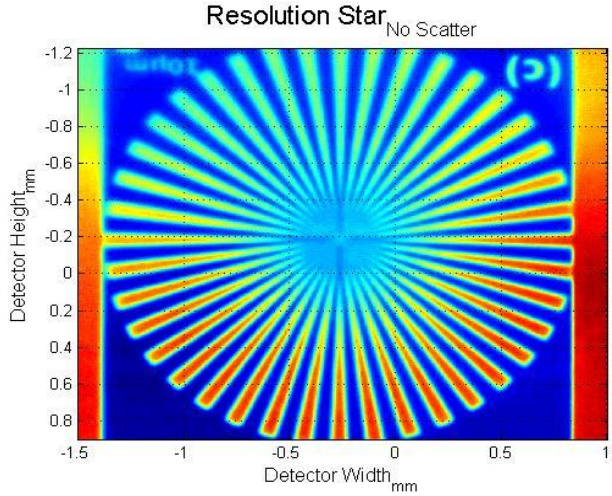

Figure 12: Resolution Star for Qualitative Analysis

Image Degradation from Scatter

The system was altered to operate at f/45. The aperture stop was set to 1.0 [mm]. This changed the frequency cut-off to 33.2 [cycles/mm]. Milk was then added to the tank in increments of 15 [ml].

Edge Response: Evaluations of the edge response under scattering conditions acted as expected. Noise reduction was a top priority after results from ideal edge response data collection revealed strong noise effects. These results were difficult to collect and even more difficult to process. The most favorable lighting condition for uniformity was determined to occur under back-lit conditions. However, this limited the irradiance of the edge object. By decreasing the total irradiance reaching the object, the signal to noise ratio deteriorated. The light irradiance counts from the object registered unmeasurable amounts after 0.8% milk by volume was achieved. The Tank Illumination System produced scatter that dominated the total irradiance in the image. The following figures show the image quality degrading with increasing scatter in the tank.

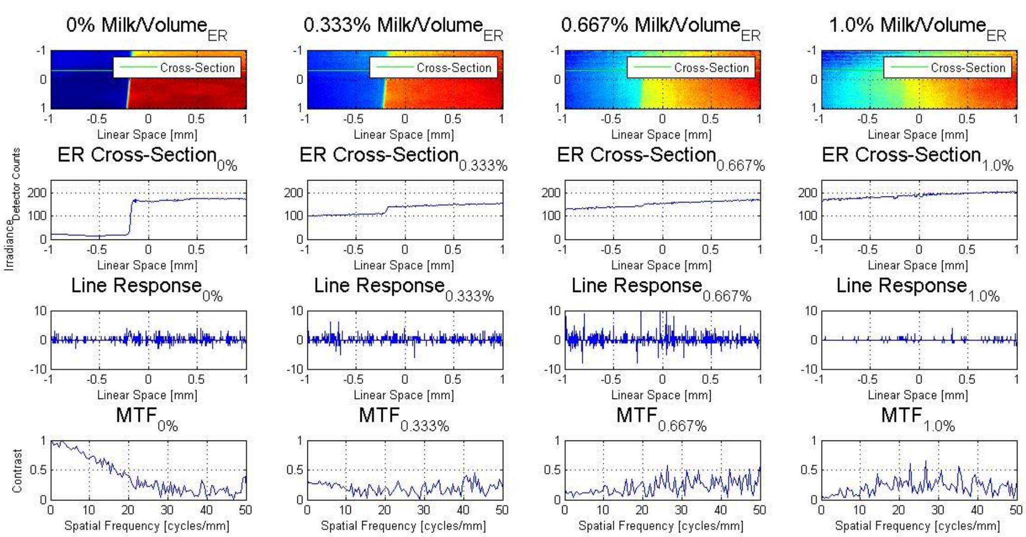

Figure 13: Edge Response Degradation as a Function of Increased Milk

PSF: The experimental set-up was recreated for an f/30 system. The increase in entrance pupil diameter was expected to allow more scattered light to enter the optical system. A frequency cut-off of 50 [cycles/mm] was expected based on the system design. Also, the diode laser was set to operate at 10% of maximum while the camera shutter was increased to allow longer integration time. The results were as expected. As milk was added to the tank, the light scattering from the tank into the system increased, as seen by the background levels in the image. The following figure shows the raw data for the PSF and calculated MTF. A noticeable "floor" in the results is seen from the uniform scattered light entering the system. Post processing removed the floor of scattered light from the original experimental data and regenerated the experimental MTF without scatter. By removing the scattered light, the MTF is only reliant on the light energy under the Airy Pattern. Without removing the scatter light, the MTF will be dominated by this scattered light. This was done by removing counts that were added uniformly across the detector. These results are plotted against the ideal MTF for a theoretical f/30 system. The blue curve on the plot represents the light present across the detector including that scattered in uniformly. The red curve represents the results after the removal of the scattered light.

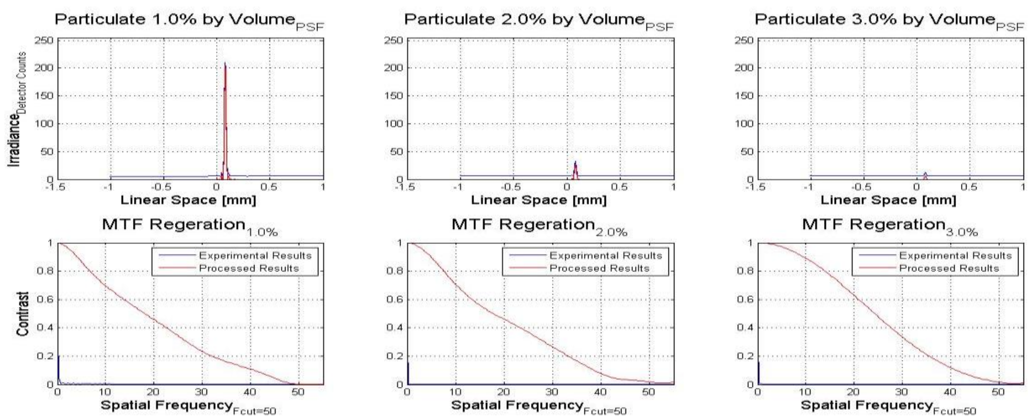

Figure 14: Influence of Scatter on PSF and MTF: MTF Regeneration

Star Target: This set-up was identical to the above edge response set-up that imaged the resolution target using an f/30 system. This set-up utilized the front-lit illumination method as the object was printed onto a sheet of computer paper. The image quality of the star degraded as the irradiance from the tank dominated the total irradiance reaching the detector. The amount of scatter required to completely degrade the image was greater than that of the Edge Response utilizing the back-lit illumination system. The image was no longer detectable with the human eye after 1.0% milk by volume was added to the tank. The following images show the degradation in image quality that occurred as a result of increasing scattered light into the system.

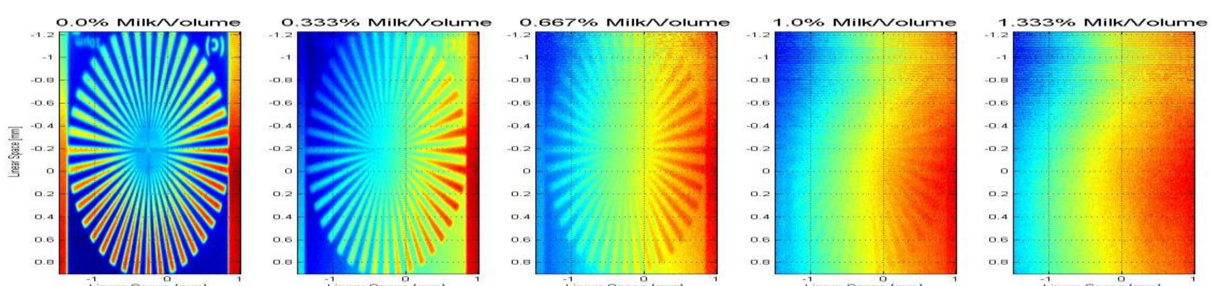

Figure 15: Resolution Star Degradation as a Function of Increased Milk by Volume

System Image Regeneration from Polarization

This system set-up was altered from the previous set-ups by the introduction of a polarizer. All other system features remained constant from the previous section. Data was collected for each polarization orientation as milk was added to the system. Images were collected while the polarizer was positioned in front of the optical system. The polarizer was positioned at angles of 0º, 25º, 45º, and 90º. Research by Pomozi was used to theoretically predict that an angle of 25º would result in blocking the majority of the polarized light from the Tank Illumination System.

PSF: The following figure illustrates the effects of changing the polarizer angle while imaging a point source through simulate scatter. As the polarization angle changes the laser light able to pass through the polarizer changes. The irradiance from the point source was decreased to reduce the dominating effects that occurred over the scatter light. By doing this, the scattered light was able to affect the resulting image.

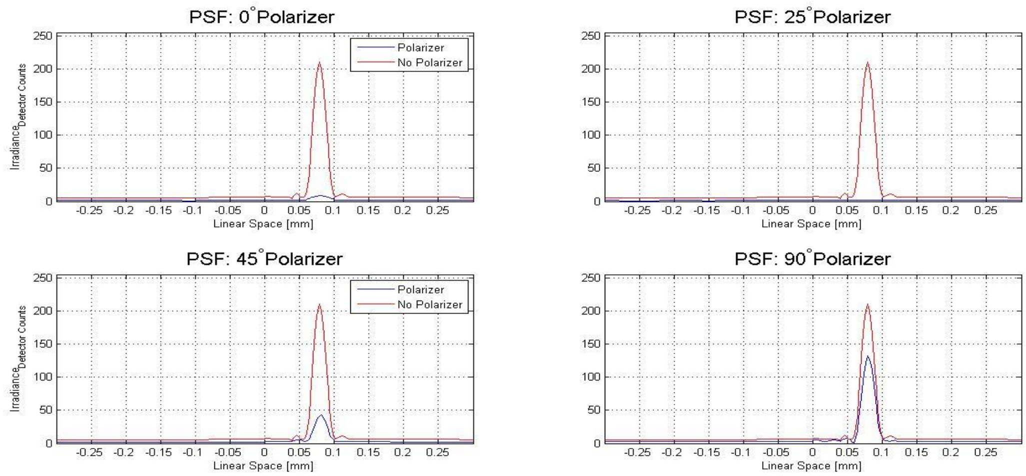

Figure 16: PSF at 1.0% Milk by Volume as a Function of Polarizer Angle

Edge: Upon evaluating the polarizer effect in the experimental process, scattered light from the tank illumination system showed characteristics of polarization. This can be concluded because the irradiance from the tank changes uniformly across the detector with respect to the polarizer angle change. The scattered light into the system from the tank has proven to uniformly increase the counts per pixel across the detector. This uniform increase appears in the data as a false floor of counts that resembles DC offset. Seeing these values change when the polarizer angle was altered, validated the assumption that scatter from the tank produced partially polarized light. Figure 17 shows the effects of adding a polarizer to the system. Each image compares the system operating without a polarizer present to each of the polarizer's angles when 0.333% milk by volume has been added to the tank. Each image in series shows an increase in polarizer angle with the maximum angle being 90º.

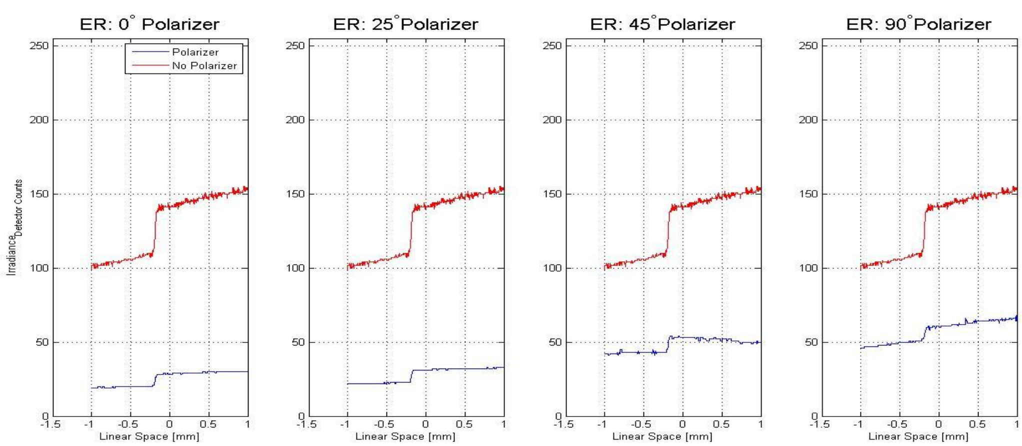

Figure 17: ER at 0.333% Milk by Volume as a Function of Polarizer Angle

Star Target: The resolution target was used for qualitative analysis of the system performance. The overall experimental data collection process was conducted until the target was no longer visually present in the resulting image. The resolution target was imaged with the same change in polarizer angle as the PSF and Edge Response. The following figure shows the degradation in image equality as an effect of polarization which was maximized at a linear polarization angle of 0º.

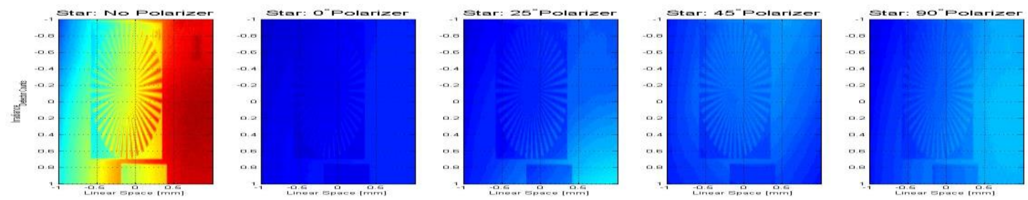

Figure 18: Resolution Target at 0.333% Milk by Volume as a Function of Polarizer Angle

Since a minimal amount of object light enters the system, the small amount of milk by volume added to the tank yields image degradation. The polarizer angle of 25º had the strongest effect on blocking irradiance from scatter. As the percentage of milk in the tank increased, image degradation increased until the object was no longer present. In this instance, the addition of the polarizer to the optical system resulted in slight visual regeneration at polarizer angle 25º.

VIII. Conclusion

After collecting and processing experimental data, several conclusions can be drawn from the results. By the known position of the source overhead and the angle of polarized light that was produced from the tank, the illumination of the tank was dominated by Rayleigh scattering. The uniform light added to the image was reduced with a polarizer angle of 25º, which suggests that this orientation of polarization is occurring from the scatter. The goal to create Rayleigh scattering was achieved. The assumption that the particles in the milk would be small enough to produce Rayleigh scattering light was justified. Also, the resolution target image regeneration occurred when the polarizer was positioned at 25º suggesting that polarization effects from the tank were highest in the 25º. By using the polarizer to block irradiance from scatter, light from the resolution target was visible.

Another achieved goal was the degradation of image quality for each of the three object sources. The tank was positioned along the optical axis between the object and imaging system. This was done to simulate atmospheric conditions. The particles in the tank sent scattered light into the imaging system while also scattering object light. The combination of these irradiance altering properties produced degraded images with minimal milk by volume added. The edge and resolution objects were almost completed degraded by 1.0% milk by volume added to the tank. The point source was not as easily degraded; however, total image degradation occurs near 3.0% milk by volume.

Finally, the goal of comparing calculated MTF by an edge source and from a point source was not met. Scattered light produced by the tank illumination system dominated the total irradiance reaching the detector. This did not allow for accurate calculations of the MTF. However, the MTF calculated by using the point source object revealed that the MTF did not vary much from the theoretically expected results. This result highlights an issue that was not considering in the initial design of the system. By using the resolution star target, visual analysis showed that the image degraded with the presence of tank illumination scatter into the system. While the point source MTF showed that the MTF for the system was not changing as a result of the scattered light. It can be concluded that in certain situations the MTF of a system does not accurately address the image quality that will be produced. This unexpected result gives insight to the possibility that MTFs are not always the best measure of system performance.

IX. Future Work

Slight changes to the experimental process would allow for more successful results. For the PSF, the system adjustments necessary to allow scatter into the system would be adjusted further to balance the effects of the object source light and the polarized light scatter by the tank.

Future work with the Edge Response would concentrate on decreasing the noise. Under the current experimental set-up, uniform illumination was not possible. The sources used did not produce the uniform illumination required to properly characterize the MTF response from the edge function. By experimenting with different sources and experimenting with the differences between back and front-lit illumination, the results can be changed dramatically.

The Star target was not quantitatively analyzed during the course of the experiment. Future work would allow for the creation of an algorithm that could analyze the frequency at which contrast dropped below a threshold. This would result in greater quantitative knowledge of the optical system performance rather than that of visual performance evaluation.

After experiencing difficulties in using the haze reduction calculations to regenerate object irradiance information from the dominating scattered irradiance, this portion of the experiment would be adjusted for greater distance between object and imaging system. This would allow the effects of atmospheric transmission to affect both the object irradiance and scattered light equally. Also, a better understanding of the simulated “atmospheric” conditions (β) used for the calculation would yield better results.

References

Arai, K. (2013). Comparison between Rayleigh and Mie Scattering Assumptions for Z-R Relation and Rainfall Rate Estimation with TRMM/PR Data. International Journal of Advanced Research in Artificial Intelligence.

Coulter, B. Milk Fat Size Distribution by Laser Diffraction. (n.d.). Retrieved May 9, 2015, from https://www.beckmancoulter.com/wsrportal/bibliography?docname=BCPCS002_LE.pdf

Gaskill, J. (1978). Linear systems, Fourier Transforms, and Optics. New York: Wiley.

Greivenkamp, J. (2004). Field Guide to Geometrical Optics. Bellingham, Wash.: SPIE Press.

Konnen, G., & Stork, D. (1985). Polarized Light in Nature. Physics Today, 95-95.

Manset, N. (n.d.). Polarization in Light. Retrieved 2015, from http://www.cfht.hawaii.edu/~manset/PolarizationLightIntro.ppt.

Mansuripur, M. (2011). Field, Force, Energy & Momentum in Classical Electrodynamics. Oak Park, IL: Bentham Science.

Pomozi, I., Horváth1, G., & Wehner, R. (2001). How the clear-sky angle of polarization pattern continues underneath clouds: Full-sky measurements and implications for animal orientation. The Journal of Experimental Biology , (204).

Schechner, Y., Narasimhan, S., & Nayar, S. (2003). Polarization-Based Vision Through Haze. Applied Optics, 42(3).

Schechner, Y., Narasimhan, S., & Nayar, S. (2001). Removing Weather Effects from Monochrome Images. Institute of Electrical and Electronics Engineers, 2.

Schwiegerling, J. (2004). Field Guide to Visual and Ophthalmic optics. Bellingham, Wash.: SPIE Press.

Appendix A: List of Figures:

Appendix B: Table of Equations:

1. Transmission (Schechner, 2003)
2. Airlight (Schechner, 2003)
3. Polarization (Schechner, 2003)
4. Object Source Irradiance (Schechner, 2003)
5. Define Total Irradiance by Polarization (Schechner, 2003)
6. Redefine Airlight by Polarization (Schechner, 2003)
7. Physical Airlight and Object Source (Schechner, 2003)
8. Physical Object Source Transmission Removal (Schechner, 2003)
9. Defining Scatter: Particle Radius over Wavelength
10. Strehl Ratio
11. Modulation Transfer Function
12. Fourier Transform of Cylinder Function
13. F-Number Work / D_{airy} / Frequency Cut-Off
14. Sampling Rate & Nyquist Frequency

Appendix C: Bill of Materials

	Part	Part Number	Qty	Cost	Total
1	Illumination Bulb	Sylvania 16751 - 80PAR38/HAL/S/WFL50	2	$9.19	$18.38
2	Len Elements (1)	AC254-030-B - f=45.0 mm, Ø1" Achromatic Doublet	1	$85.50	$85.50
3	Iris	SM1D25 - SM1 Lever-Actuated Iris Diaphragm (.8-25 mm)	1	$86.70	$86.70
4	Detector	Point Gray FL3-U3-32S2M-CS - Serial #: 14462850	1	$725.00	$725.00
5	NIR Filter	NIR Band Filter: 715-1000nm - SKU: 102400167	1	$25.00	$25.00
6	Lens Mount	25.4mm Diameter, C-Mount Thin Lens Mount Stock No. #56-353	1	$73.00	$73.00
7	Filter Mount	25.4mm Diameter, C-Mount Thin Lens Mount Stock No. #56-353	1	$73.00	$73.00
8	Extra	Unplanned purchases 10% Total		$108.66	-
		Total Adjusted Total		$1,086.58	$1,195.24